

REPORT

EXOPLANETS

A multiple planet system of super-Earths orbiting the brightest red dwarf star GJ 887

S. V. Jeffers^{1*}, S. Dreizler¹, J. R. Barnes², C. A. Haswell², R. P. Nelson³, E. Rodríguez⁴, M. J. López-González⁴, N. Morales⁴, R. Luque^{5,6}, M. Zechmeister¹, S. S. Vogt⁷, J. S. Jenkins^{8,9}, E. Pallé^{5,6}, Z. M. Berdiñas⁸, G. A. L. Coleman^{3,10}, M. R. Díaz⁸, I. Ribas^{11,12}, H. R. A. Jones¹³, R. P. Butler¹⁴, C. G. Tinney¹⁵, J. Bailey¹⁵, B. D. Carter¹⁶, S. O'Toole¹⁷, R. A. Wittenmyer¹⁸, J. D. Crane¹⁹, F. Feng¹⁴, S. A. Shectman¹⁹, J. Teske¹⁹, A. Reiners¹, P. J. Amado⁴, G. Anglada-Escudé^{3,11,12}

The closest exoplanets to the Sun provide opportunities for detailed characterization of planets outside the Solar System. We report the discovery, using radial velocity measurements, of a compact multiplanet system of super-Earth exoplanets orbiting the nearby red dwarf star GJ 887. The planets have orbital periods of 9.3 and 21.8 days. Assuming an Earth-like albedo, the equilibrium temperature of the 21.8-day planet is ~ 350 kelvin. This temperature is within, but close to the inner edge of, the liquid-water habitable zone. We also detect an unconfirmed signal with a period of ~ 50 days, which could correspond to a third super-Earth in a more temperate orbit. Our observations show that GJ 887 has photometric variability below 500 parts per million, which is unusually quiet for a red dwarf.

At visible wavelengths, GJ 887 (HD 217987) is the brightest red dwarf in the sky and, at a distance of 3.29 pc, is the 12th closest star system to the Sun. GJ 887 is the most massive red dwarf within 6 pc of the Sun, which is close enough for a direct stellar radius measurement using interferometry (1). GJ 887's stellar parameters are listed in Table 1. Red dwarfs are amenable to radial velocity (RV) searches for temperate Earth-mass exoplanets: their low luminosity means that temperate planets have short orbital periods, and

their low stellar mass implies that Earth-mass planets can impart a reflex RV detectable with current instrumentation. Although the transit method of planet discovery efficiently detects planets because many stars can be simultaneously monitored, it will detect only planets that pass through the line of sight between Earth and the host star. Consequently, only 1 to 2% of habitable-zone planets (i.e., those with surfaces that can support liquid water) are detectable with the transit method. The RV method is necessary to achieve a complete

census of the planets orbiting our closest stellar neighbors, especially red dwarfs.

We monitored GJ 887 as part of the Red Dots #2 project. Nightly observations were taken with the High Accuracy Radial Velocity Planet Searcher (HARPS) (2) for 3 months. We also obtained contemporaneous photometric observations (3). Regular nightly sampling combined with photometric observations mitigates against false-positive exoplanet detections caused by intrinsic stellar variability and other sources of correlated noise. We supplement our data with >200 archival observations from HARPS, the Planet Finder Spectrograph (PFS) (4), the High-Resolution Echelle Spectrometer (HIRES) (5), and the University College London Echelle Spectrograph (UCLES) (6), spanning nearly 20 years (3). We used photometry from various ground-based observatories and the Transiting Exoplanet Survey Satellite (TESS) spacecraft (7). Tables S3 and S4 list all the data we used.

We searched for a candidate planet by adding a (circular) Keplerian orbit test signal to a base model and measuring the improvement in the logarithm of the likelihood statistic (3). The base model is composed of an offset and an instrumental jitter added to the measurement uncertainties for each dataset. We used this to generate log-likelihood periodograms for both the RV and photometric data and then searched for signals by plotting the increase in the log-likelihood statistic against test period (Fig. 1). The highest peaks were evaluated for statistical significance (8, 9). We recursively added additional planet test signals, adjusting all the parameters to maximize the likelihood

¹Institut für Astrophysik, Georg-August-Universität, 37077 Göttingen, Germany. ²School of Physical Sciences, The Open University, Milton Keynes MK7 6AA, UK. ³School of Physics and Astronomy, Queen Mary University of London, London E1 4NS, UK. ⁴Instituto de Astrofísica de Andalucía, Consejo Superior de Investigaciones Científicas, 18008 Granada, Spain. ⁵Instituto de Astrofísica de Canarias, 38205 La Laguna, Tenerife, Spain. ⁶Departamento de Astrofísica, Universidad de La Laguna, 38206 La Laguna, Tenerife, Spain. ⁷Lick Observatory, University of California, Santa Cruz, Santa Cruz, CA 95064, USA. ⁸Departamento de Astronomía, Universidad de Chile, 7591245 Santiago, Chile. ⁹Centro de Astrofísica y Tecnologías Afines, 7591245 Santiago, Chile. ¹⁰Physikalisches Institut, Universität Bern, 3012 Bern, Switzerland. ¹¹Institut de Ciències de l'Espai, Consejo Superior de Investigaciones Científicas, Campus Universitat Autònoma de Barcelona, E-08193 Bellaterra, Spain. ¹²Istitut d'Estudis Espacials de Catalunya, E-08034 Barcelona, Spain. ¹³Centre for Astrophysics Research, University of Hertfordshire, Hatfield AL10 9AB, UK. ¹⁴Earth and Planets Laboratory, Carnegie Institution for Science, Washington, DC 20015, USA. ¹⁵Exoplanetary Science at University of New South Wales, School of Physics, University of New South Wales, Sydney, NSW 2052, Australia. ¹⁶Centre for Astrophysics, University of Southern Queensland, Springfield Central, QLD 4300, Australia. ¹⁷Australian Astronomical Optics, Macquarie University, North Ryde, NSW 2113, Australia. ¹⁸Centre for Astrophysics, University of Southern Queensland, Toowoomba, QLD 4350, Australia. ¹⁹The Observatories of the Carnegie Institution for Science, Pasadena, CA 91101, USA.

*Corresponding author. Email: sandrajefers.astro@gmail.com

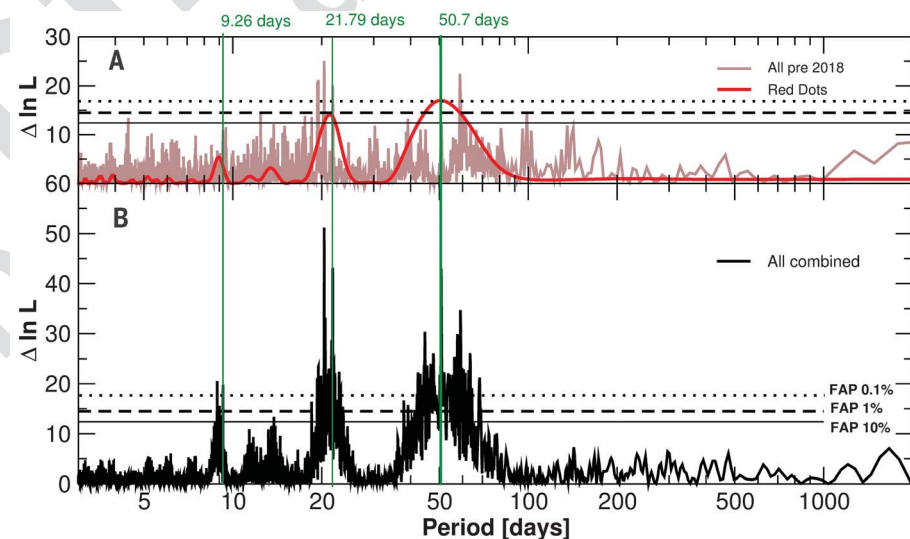


Fig. 1. Periodograms of the RV data. (A) The log-likelihood ($\Delta \ln L$) periodogram obtained separately for all RV data before 2018 (brown) and the Red Dots #2 campaign (red). (B) the same search for a first signal when combining all the RV observations together. The vertical green lines indicate our derived model periods for planets b and c and the candidate planet d. The horizontal dashed lines in both panels indicate the false alarm probability (FAP) values.

of all planet signals and the parameters of the base model. We continued this iterative process until no signals below a threshold of 0.1% false-alarm probability were found in the time series (fig. S1). We detected periodic signals at 9.3, 21.8, and 50.7 days (Fig. 1B) and verified them using several independent fitting procedures and algorithm implementations (3). The regular sampling of the Red Dots #2 dataset helped to disentangle the signals under investigation (Fig. 1A).

Stellar magnetic activity can induce an asymmetric distortion of the spectral lines, shifting the measured line center and consequently inducing an apparent RV shift, which may appear as a false-positive exoplanet at the stellar rotation period (10). The rotation period of GJ 887 is unknown, so we searched for periodicities in the photometric data (3). The archival data from 2002–2004 show an ~200-day period, but this period was undetectable in the 2018 quasi-simultaneous photometric observations because the time span is too short. Our analysis of the TESS photometry shows very low intrinsic variability, with a semi-amplitude of 240 parts per million. It is unclear whether this is caused by systematic effects, known to affect the TESS observations, but we use this value as an upper limit to the intrinsic variability

of GJ 887. The TESS variability can be explained by one starspot, or a group of starspots, with a total diameter of 0.3% of the stellar surface, indicating that GJ 887 is slowly rotating with very few surface brightness inhomogeneities (11). GJ 887 is less magnetically active than most stars with the same effective temperature, as demonstrated by: the very low starspot coverage; low photometric variability; the activity metric derived from stellar Ca II H and K lines, $\log(R'_{HK}) = -4.805$ (12); and the very low H α activity (13).

The RV signals are detected in the Red Dots #2 HARPS data alone (Fig. 1A), so we investigated additional spectral signatures of stellar magnetic activity using this dataset. We extracted a time series of the flux in the cores of the Na I D, H α , and H β lines; and calculated the S-index, which is the ratio of flux in the cores in the Ca II H and K lines compared with the continuum (3). The S-index and Na I D lines both show a weak signal at about 55 days, whereas the H α and H β lines show a weak signal at 38 days (fig. S5). These differing periodicities could reflect time scales of various stellar activity processes on the star, and despite being low in amplitude, they make a planetary origin for RV signals in the 30- to 60-day domain less certain. None of these activ-

ity periodicities are close to the RV signals at 9.3 and 21.8 days, but they do make the RV signal at 50.7 days questionable.

Correlated noise, for example, that caused by stellar activity, can be assessed using the covariances between observations. To further test the planetary origin of the detected RV signals, we fitted maximum likelihood model functions using two planet models with and without Gaussian processes (GPs) (3). All of the models including GPs improved the fit to the data compared with those without, and the amplitude of the signals with periods of 9.3 and 21.8 days remained unchanged within their 1σ uncertainty. The modeling of the correlated noise using GPs therefore does not affect these two signals. However, the significance of the third signal drops substantially when including a GP in the model, casting further doubts on its Keplerian nature. Table S4 lists the derived values and statistics from these models.

We conclude that the two signals with orbital periods of 9.3 and 21.8 days correspond to two exoplanets, planets b and c, respectively. The minimum masses of these planets (m_p) are 4.2 ± 0.6 and 7.6 ± 1.2 Earth masses (M_\oplus), which makes them two super-Earth exoplanets with orbital semimajor axes (a_p) of 0.068 and 0.120 astronomical units (au). The inner

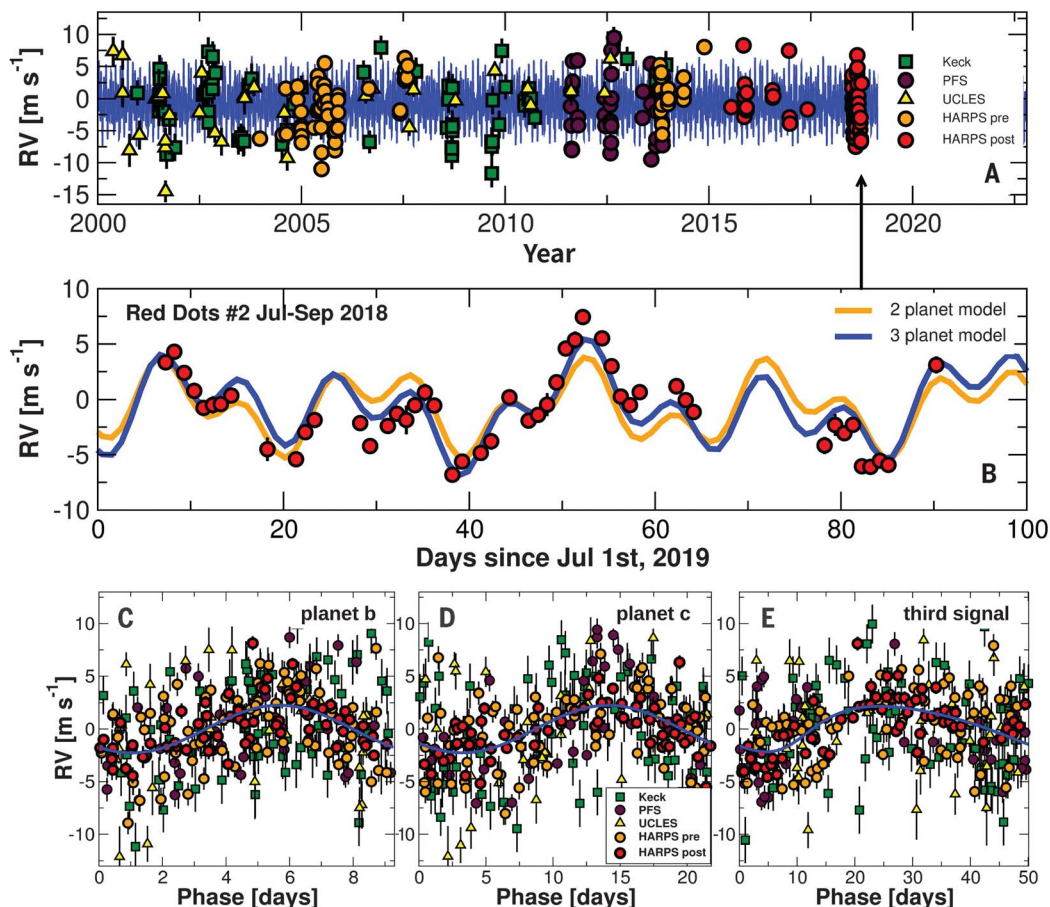


Fig. 2. Time series of radial velocity measurements. All RV measurements are shown, with the instruments used indicated in the legend. “HARPS pre” and “HARPS post” refer to data collected before and after an instrument upgrade, respectively. **(A)** Radial velocity measurements over 18 years using all instruments. The best-fitting model with three Keplerian signals is shown with a solid blue line. **(B)** Zoom in on area indicated with arrow in (A), showing the Red Dots #2 observations. The three-planet model is shown with a solid blue line, and the two-planet model with a solid orange line. It is uncertain whether the ~50-day signal has a planetary origin, but three periodic modulations are required to fit the observations. **(C to E)** The data from (A), folded on the periods of each candidate signal, after subtracting the other signals. The best-fitting model is shown as a solid blue line.

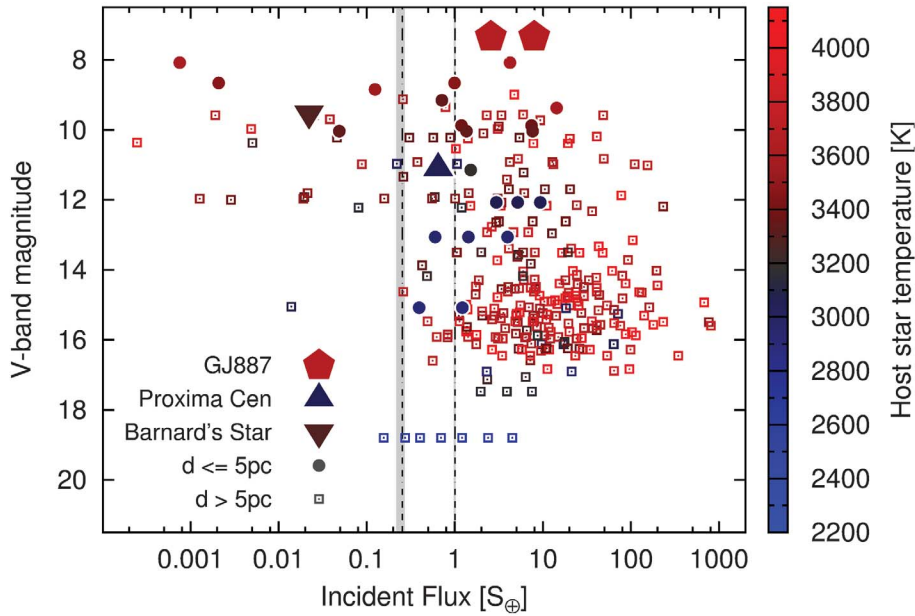


Fig. 3. The incident flux (insolation) of planets orbiting M dwarf stars. The dashed vertical lines delimit the habitable zone around GJ 887 for the maximum greenhouse planetary atmosphere (left) and the runaway greenhouse planetary atmosphere (right) (23). The solid vertical gray lines indicate the range of limits for the host stars of all planets plotted; these stars have T_{eff} ranging from 2400 to 4150 K (see color bar). GJ 887 b and GJ 887 c are indicated by the large red pentagons. Proxima Cen, Proxima Centauri; d, distance.

planet has an orbital eccentricity consistent with zero (Fig. 2), but the outer planet is more likely to have a small nonzero eccentricity (Fig. 3). We regard the third signal at ~ 50 days (compare Fig. 2) as dubious and likely related to stellar activity. The fits to our two-planet model and the two-planet + third signal model are shown in Fig. 2.

The long-term dynamical stability of the orbits can also be used to test the physical plausibility of the system and investigate whether it contains unusual configurations such as dynamical resonances. We performed a dynamical stability study (3) using the software package MERCURY6 (14). We find that all two-planet solutions are stable even if eccentricities are allowed to vary. The ratio of periods of these two planets is close to 7:3, but the simulations do not support the presence of a dynamical resonance, as there is an absence of oscillating orbital alignment variations (15). However, we find that the system must be in a dynamically active state, driving oscillatory changes in the eccentricities of both planets. These interactions produce very regular variations, supporting the hypothesis that the two-planet configuration is dynamically stable on very long time scales. For a putative system with three planets, only $\sim 25\%$ of the 1000 best-fitting models would

F2
F3

Table 1. Stellar parameters for GJ 887 and parameters for planets b and c. The top half of the table lists parameters for GJ 887: the parallax in milliarcseconds (mas), distance in parsecs (pc), V- and G-band magnitudes, stellar mass in solar masses (M_{\odot}), metallicity relative to the Sun [Fe/H], luminosity and radius in solar units, projected rotational velocity ($v \sin i$), and surface gravity $\log g$. The stellar mass was computed using a mass-radius relation (26). The bottom half of the table lists parameters for planets b and c: S_{eff} is the incident flux from GJ 887 in units of the incident flux on Earth from the Sun, and T_{eq} is the equilibrium temperature of the planet.

Parameter	Value	Reference
Spectral type	M1V	(27)
Parallax (mas)	304.2190 ± 0.0451	(28)
Distance (pc)	3.2871 ± 0.0005	
Magnitude	$V = 7.34, G = 6.522$	(28)
Mass (M_{\odot})	0.489 ± 0.05	
[Fe/H]	-0.06 ± 0.08	(27)
T_{eff} (K)	3688 ± 86	(27)
Luminosity (L_{\odot})	0.0368 ± 0.004	(27)
Radius (R_{\odot})	0.4712 ± 0.086	(1, 29, 30)
$v \sin i$ (km s^{-1})	2.5 ± 1.0	(31)
$\log R_{\text{HK}}$ mean	-4.805 ± 0.023	(12)
$\log(\text{age}/\text{years})$	9.46 ± 0.58	(27)
$\log g$	4.78	(32)
	GJ 887 b	GJ 887 c
K_p (m s^{-1})	$2.1^{+0.3}_{-0.2}$	2.8 ± 0.4
P_p (d)	9.262 ± 0.001	$21.789^{+0.004}_{-0.005}$
m_p (M_{\oplus})	4.2 ± 0.6	7.6 ± 1.2
a_p (au)	0.068 ± 0.002	0.120 ± 0.004
$S_{\text{eff},p}$ ($S_{\text{eff},\oplus}$)	7.95 ± 0.2	2.56 ± 0.2
T_{eq} (K)	468	352

be dynamically stable over 10^5 years, but this is mostly due to the poorly constrained eccentricities. Given that the observations only provide upper limits on the eccentricities, we investigated orbits that are assumed to be initially circular (initial zero eccentricities). Even in this three-planet case, >99% of configurations were found to be stable, meaning that the presence of a third planet cannot be ruled out using dynamic stability considerations.

The separations between the planets, in units of their spheres of gravitational influence (Hill radii), are ~ 19.1 for planets b and c and ~ 17.2 for planets c and d (if planet d is real and has a mass of $8.3 M_{\oplus}$); these values are consistent with the system having undergone dynamical relaxation (16). Dynamical relaxation in systems of super-Earths results in $\sim 80\%$ of planets having orbital eccentricities $e_p \leq 0.1$, with the remaining 20% having $e_p \leq 0.3$ (17). We examined the expected tidal evolution of GJ 887 b using analytical methods (18, 19), finding that the tidal circularization time scale of GJ 887 b is a few billion years for an assumed tidal dissipation parameter $Q'_p = 1000$. This is consistent with our observation that GJ 887 b's orbit is almost circular.

The multiplanet super-Earth system around GJ 887 is consistent with recent planet formation models (20, 21). These models typically form chains of multiple planets trapped in mean-motion resonances that then migrate into orbits close to the central star. Depending on where the initial planets formed in the protoplanetary disc, they could have accreted either large amounts of water ice or just dry rocky silicates. As such, the planets may be either water-rich or water-poor. At the end of the gas disc lifetime, the resonant chains of planets can remain stable, yielding systems similar to the seven-planet TRAPPIST-1 planetary system (22), or they can become unstable, leading to collisions between planets and thus a nonresonant configuration (20). The GJ 887 planetary system appears to be more consistent with the latter scenario of unstable evolution. The presence of dynamical resonances can be very sensitive to the existence or absence of additional planets. Consequently, if the third signal at 50.7 days is real or if additional planets exist, this may result in a more resonant system.

We used standard methods (23) to calculate the distances from GJ 887 within which planets could support liquid water on their surfaces [the star's habitable zone (HZ)] and found that it extends from ~ 0.19 to 0.38 au. With an a_p of 0.120 ± 0.004 , GJ 887 c is closer to its host star than the HZ but near the inner edge. If the ~ 50 -day signal is planetary in origin, it corresponds to a super-Earth in GJ 887's HZ. Assuming an albedo, α , similar to Earth's ($\alpha = 0.3$), the equilibrium temperature, T_{cep} , of planets b and c would be 468 and 352 K, respectively.

Their incident energy fluxes from the star (the insolation S) are 7.95 and 2.56 times the Sun's insolation on Earth. Figure 3 shows the insolation of known planets orbiting M-type red dwarfs as a function of host star apparent magnitude. GJ 887 has the brightest apparent magnitude of any known M dwarf planet host. This brightness, combined with the high photometric stability of GJ 887, exhibited in the TESS data, and the high planet-star brightness and radius ratios, make these planets potential targets for phase-resolved photometric studies, especially in emission (24). Spectrally resolved phase photometry has been shown to be sensitive to the presence of an atmosphere and molecules such as CO_2 (25).

REFERENCES AND NOTES

1. T. S. Boyajian et al., *Astrophys. J.* **757**, 112 (2012).
2. M. Mayor et al., *Messenger* **114**, 20–24 (2003).
3. See supplementary materials.
4. J. D. Crane et al., *Proc. SPIE* **7735**, 773553 (2010).
5. S. S. Vogt et al., *Proc. SPIE* **2198**, 362–375 (1994).
6. F. Diego, A. Charalambous, A. C. Fish, D. D. Walker, *Proc. SPIE* **1235**, 562–576 (1990).
7. G. R. Ricker et al., *J. Astron. Telesc. Instrum. Syst.* **1**, 014003 (2015).
8. R. V. Baluev, *Mon. Not. R. Astron. Soc.* **393**, 969–978 (2009).
9. I. Ribas et al., *Nature* **563**, 365–368 (2018).
10. S. V. Jeffers et al., *Mon. Not. R. Astron. Soc.* **438**, 2717–2731 (2014).
11. J. R. Barnes et al., *Astrophys. J.* **812**, 42 (2015).
12. S. Boro Saikia et al., *Astron. Astrophys.* **616**, A108 (2018).
13. S. V. Jeffers et al., *Astron. Astrophys.* **614**, A76 (2018).
14. J. E. Chambers, *Mon. Not. R. Astron. Soc.* **304**, 793–799 (1999).
15. M. Perryman, *The Exoplanet Handbook* (Cambridge Univ. Press, ed. 2, 2018).
16. B. Pu, Y. Wu, *Astrophys. J.* **807**, 44 (2015).
17. S. T. S. Poon, R. P. Nelson, S. A. Jacobson, A. Morbidelli, *Mon. Not. R. Astron. Soc.* **491**, 5595–5620 (2020).
18. I. Dobbs-Dixon, D. N. C. Lin, R. A. Mardling, *Astrophys. J.* **610**, 464–476 (2004).
19. P. P. Eggleton, L. G. Kiseleva, P. Hut, *Astrophys. J.* **499**, 853–870 (1998).
20. G. A. L. Coleman, R. P. Nelson, *Mon. Not. R. Astron. Soc.* **457**, 2480–2500 (2016).
21. M. Lambrechts et al., *Astron. Astrophys.* **627**, A83 (2019).
22. M. Gillon et al., *Nature* **542**, 456–460 (2017).
23. R. K. Kopparapu et al., *Astrophys. J.* **787**, L29 (2014).
24. E. M. R. Kempton et al., *Publ. Astron. Soc. Pac.* **130**, 114401 (2018).
25. I. A. G. Snellen et al., *Astron. J.* **154**, 77 (2017).
26. A. Schweitzer et al., *Astron. Astrophys.* **625**, A68 (2019).
27. A. W. Mann, G. A. Feiden, E. Gaidos, T. Boyajian, K. von Braun, *Astrophys. J.* **804**, 64 (2015).
28. Gaia Collaboration, *Astron. Astrophys.* **616**, A1 (2018).
29. D. Ségransan, P. Kervella, T. Forveille, D. Queloz, *Astron. Astrophys.* **397**, L5–L8 (2003).
30. B.-O. Demory et al., *Astron. Astrophys.* **505**, 205–215 (2009).
31. M. K. Browning, G. Basri, G. W. Marcy, A. A. West, J. Zhang, *Astron. J.* **139**, 504–518 (2010).
32. M. Rabus et al., *Mon. Not. R. Astron. Soc.* **484**, 2674–2683 (2019).
33. R. P. Butler et al., *Astron. J.* **153**, 208 (2017).

ACKNOWLEDGMENTS

We thank P. A. Peña Rojas for contributing results using the EMPEROR code. This work is based on observations collected at the European Organisation for Astronomical Research in the Southern Hemisphere under ESO programmes 0101.C-0516, 0101.C-0494, and 0102.C-0525. This Report includes data gathered with the 6.5-m Magellan Telescopes located at Las Campanas Observatory, Chile. Photometric data were collected with the robotic 40-cm telescope ASH2 at the SPACEOBS observatory (San Pedro de Atacama, Chile) operated by the Instituto de Astrofísica de Andalucía (IAA). This paper includes data collected with the

TESS mission, obtained from the Mikulski Archive for Space Telescopes (MAST) data archive at the Space Telescope Science Institute (STScI). Funding for the TESS mission is provided by the NASA Explorer Program. STScI is operated by the Association of Universities for Research in Astronomy, Inc., under NASA contract NAS 5-26555. **Funding:** S.V.J. acknowledges the support of the German Science Foundation (DFG) Research Unit FOR2544 “Blue Planets around Red Stars” project (JE 701/3-1) and DFG priority program SPP 1992 “Exploring the Diversity of Extrasolar Planets” (RE 1664/18). J.R.B. and C.A.H. acknowledge support from STFC Consolidated Grants ST/P000584/1 and ST/T000295/1. R.P.N. was supported by STFC Consolidated Grant ST/P000592/1. E.R., M.J.L.G., N.M., and P.J.A. acknowledge support from the Spanish Agencia Estatal de Investigación through projects AYA2017-89637-R, AYA2016-79425-C3-3-P, ESP2017-87676-C5-2-R, and ESP2017-87143-R and the Centre of Excellence “Severo Ochoa” Instituto de Astrofísica de Andalucía (SEV-2017-0709). E.P. acknowledges support from the Spanish Agencia Estatal de Investigación PGC2018-098153-B-C31 and ESP2016-80435-C2-2-R. Z.M.B. acknowledges funds from CONICYT/FONDECYT POSTDOCTORADO 3180405. G.A.L.C. acknowledges support from the Swiss National Science Foundation. M.R.D. acknowledges support of CONICYT/PFCHA-Doctorado Nacional 21140646, Chile. I.R. acknowledges support from the Spanish Ministry of Science and Innovation and the European Regional Development Fund through grants ESP2016-80435-C2-1-R and PGC2018-098153-B-C33 and the Generalitat de Catalunya/CERCA program. H.R.A.J. acknowledges support from the U.K. Science and Technology Facilities Council grant ST/M001008/1. C.G.T. is supported by Australian Research Council grants DP0774000, DP130102695, and DP170103491. J.T. was supported by NASA through Hubble Fellowship grant HST-HF2-51399.001 awarded by the Space Telescope Science Institute, which is operated by the Association of Universities for Research in Astronomy, Inc., for NASA, under contract NAS5-26555. G.A.E. is supported by the Ministerio de Ciencia, Innovación y Universidades Ramón y Cajal fellowship RYG-2017-22489 and by the Science and Technology Facilities Council grant number ST/P000592/1.

Author contributions: S.V.J. led the observing proposal, team coordination, participated in the data analysis, and wrote the manuscript. S.D. led the data analysis and contributed to the writing of the manuscript. J.R.B. participated in the writing of the observing proposal, simulations, and reviewing manuscript. C.A.H. participated in the writing of the observing proposal, final consistency checks, and writing of the manuscript. R.P.N.: Contributed the discussion of planetary dynamics and manuscript review. E.R.: ASH2 photometry, coordination of photometric observations, data analysis. M.J.L.G.: ASH2 photometry data reduction. N.M.: ASH2 photometry observer. R.L., M.Z., S.S.V., and J.J. ran the blind tests, data analysis, and manuscript review. E.P.: Data analysis and manuscript review. Z.M.B. and M.R.D.: Contribution of HARPS data and manuscript review. G.A.L.C.: Contributed to the discussion of planet formation and manuscript review. I.R., H.R.A.J., A.R., and P.J.A.: Writing and review of manuscript. R.P.B.: AAT/PFS data collection and analysis. C.G.T., J.B., B.D.C., S.O.T., and R.W. were AAT/UCLES observers and reviewed the manuscript. J.D.C., F.F., S.A.S., and J.T. were PFS observers. G.A.E.: Writing of the observing proposal, data analysis, and writing of the manuscript. **Competing interests:** There are no competing interests to declare. **Data and materials availability:** The reduced RVs and photometric data are provided in data S1. Our HARPS raw data are available in the ESO archive (<http://archive.eso.org>) under the program IDs listed in table S1. Reduced HIRES RVs were taken from (33). The UCLES data are available from the AAT archive (<https://datacentral.org.au/archives/aat/>) by searching the coordinates RA '23:05:52h', Dec '-35:51:11d', a radius of 300 arcseconds, and dates 1998–2012. The PFS spectra, our dynamical stability simulations, and our Gaussian processes fitting code are available at <https://figshare.com/s/d581c1a17536eeb813ea>. The TESS photometry was retrieved from <https://mast.stsci.edu/portal/Mashup/Clients/Mast/Portal.html>, and the All Sky Automated Survey (ASAS) photometry was retrieved from www.astrouw.edu.pl/asas/?page=aasc.

SUPPLEMENTARY MATERIALS

[science.sciencemag.org/content/\[vol\]/\[issue\]/\[page\]/suppl/DC1](https://science.sciencemag.org/content/[vol]/[issue]/[page]/suppl/DC1)
Materials and Methods
Figs. S1 to S11
Tables S1 to S7
References (34–70)
Data S1

9 August 2019; accepted 12 May 2020
10.1126/science.aaz0795